Photogrammetric Characterization of a Brownout Cloud

Philip E. Tanner
U.S. Army Joint Research Program Office, Aeroflightdynamics Directorate
NASA Langley Research Center, Hampton, VA 23681

Abstract

Brownout is a dangerous problem for rotorcraft operating in arid and dusty environments such as the current operating theaters in Iraq and Afghanistan. Although the interest in brownout has increased in the past decade, the fundamental physics that govern the shape and size of the cloud are not yet well understood. Many computational and scaled experimental studies have been performed in an attempt to further this understanding and to simulate and predict the brownout cloud formation. However, the phenomenon significantly lacks experimental data, particularly at full-scale, which is needed to help validate the brownout simulations being performed. In an effort to increase the data set needed for this validation, tests were performed at the US Army Yuma Proving Ground using photogrammetry to obtain brownout cloud data of an EH-60L Black Hawk. Particle testing was performed on a sample of sand from the landing zone to gain more understanding on the nature of the soil. The photogrammetry technique applied to obtaining data on the formation and evolution of a brownout cloud was verified in an earlier study. The data for a landing approach was examined in greater detail and enabled velocity components of points on the cloud to be determined, as well as the dimensions of structures within the cloud.

Introduction

The degraded visual environment (DVE) caused by brownout is one of the most dangerous problems existing for rotorcraft operating in arid and dusty environments[1]. Brownout, or whiteout in arctic environments, results from the high velocity of induced flow near the ground lifting up loose surface particles, which then become entrained by the downwash/outwash of the rotorcraft and produce a large cloud of dust that can quickly envelop the aircraft and cause the pilot to lose situational awareness[2-4]. An example of an aircraft encountering this is shown in Figure 1. In turn, the pilot loses visual references to the landing zone, which can cause spatial disorientation and lead to an unintended induced drift, either laterally or longitudinally, just prior to touchdown. Few aircraft can handle a sideward or rearward movement during touchdown, as this can result in contact with other aircraft or objects on the ground and/or dynamic aircraft rollover[1,5].

Due to the inherent nature of brownout, it is fundamentally a complex physical phenomenon, with a typical brownout cloud containing billions of sediment particles ranging in size from 1μm to 100μm, and can be influenced by a wide range of factors[6]. The environmental conditions present at the landing zone surface have a significant effect on the strength and duration of the brownout cloud that forms, such as the wind speed and direction and the moisture content and composition of the soil[1,6].The performance of an aircraft under brownout appears to be affected by a variety of mutually dependent aircraft parameters, such as the rotor disk loading, fuselage shape, rotor RPM, and aircraft configuration, and various blade parameters, such as the radius, chord, twist, geometry, root cutout, loading, and number[2,3,7]. The flight path of an aircraft into brownout also seems to have a considerable effect on the shape of the brownout cloud generated[3].

Figure 1. EH-60L entering brownout-induced DVE

According to the recent Aviation Technologies Safety Report by the Department of Defense, brownout and whiteout-induced DVE is the primary cause of airframe losses for the Army and accounts for half of those for Air Force rotorcraft[5]. Between 2001 and 2008, brownout and obstacle strikes accounted for 48, or 37%, of non-hostile rotorcraft losses in Iraq and Afghanistan, as well as an additional 25, or 38%, non-combat losses elsewhere[8,9]. Not all damages by brownout-induced

Presented at the American Helicopter Society 67th Annual Forum, Virginia Beach VA, 3-5 May 2011.

DVE result in airframe losses, but aircraft operating in these settings experience significantly reduced lifetimes of rotor blades, filters, engines, and other components exposed to the abrasive dust cloud[10,11]. Approximately 80% of Army brownout incidents occur during landing[12] and it is estimated that brownout costs the Army alone more than $60M per year[13], and $100M per year when all branches of the military are included[14].

Given the costs and severity of brownout-induced DVE, it has become an increasingly popular research topic within the rotorcraft community, with several computational and scaled experimental studies having been performed in recent years[6,15-20]. However, the fundamental aerodynamics governing the phenomenon remain to be fully understood, and little experimental data regarding particle transport, with respect to brownout, exists[3,16]. Advanced modeling methods focused on the prediction of the downwash and induced flow and the growth of the brownout cloud are being attempted, but these methods are still in their early stages and lack experimental data for code validation, particularly at full-scale and in relevant environments[3,6,7,21].

A data set was obtained for an EH-60L Black Hawk by using photogrammetry to track the formation and evolution of a brownout cloud during landing at the US Army Yuma Proving Ground (YPG) in the southwest Arizona desert. The photogrammetry process was previously validated against data obtained from the onboard instruments[22]. This paper focuses on one small, two-second timeframe of the brownout cloud evolution, at an increased temporal resolution than examined in the earlier study, in order to obtain a variety of cloud parameters, such as particle position, velocity and direction, and to define any noticeable structures existing in the cloud. Further understanding will help researchers validate predictive codes, obtain more accurate brownout simulations, and possibly help identify measures to protect against the dangerous phenomenon.

Photogrammetry

A photographic image is the result of a three-dimensional object's projection to two dimensions. Photogrammetry is the tool used to extract quantitative data from an image to determine the two-dimensional or three-dimensional coordinates of an object in a photograph, and it was first developed to examine topography using aerial photographs[23]. In order to find the three-dimensional coordinates of an object, multiple photographs must be taken of that object from a variety of different perspectives. Using triangulation, rays from the camera to points on an object in the image are intersected, and with a user-defined coordinate system, at least one known distance, and camera-specific parameters such as the sensor size and lens focal length known, the three-dimensional coordinates of an object in object space can be found. A schematic of this process, showing different camera positions and the rays used for triangulation, is given in Figure 2. Photogrammetry can be a high-accuracy measurement system, with claimed accuracies for some systems approaching 0.002" to 0.004" on a ten-foot object[24].

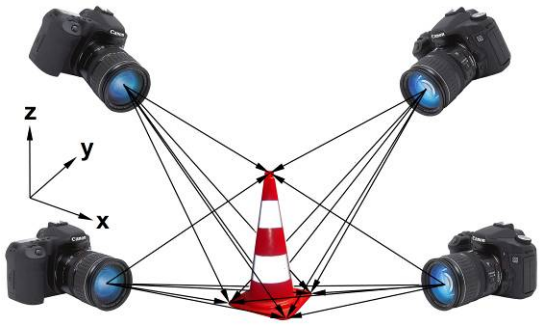

Figure 2. Schematic of photogrammetry of a cone

Validation of the photogrammetric technique was performed in order to make certain that the quantitative measurements obtained of the brownout cloud were reasonable and accurate. This was done by comparing the distances between various objects measured through photogrammetry to the same distances measured by mechanical means, along with comparing the position data determined from multiple frames of a taxi pass event to the flight-track data obtained from the onboard instruments, specifically the inertial measurement unit (IMU), embedded GPS/INS (EGI) and radar altimeter. The largest error between the mechanically-measured distances and those calculated from the photogrammetric data was about 4.5%. See Reference 22 for a more detailed description of this process.

In traditional photogrammetry, special retroreflective dots and codes are placed on and around the object(s) of interest in the images. These dots and coded targets help by forming distinct points in the images that are recognized by the photogrammetry software and facilitate easier referencing of similar points between the images. The coded targets can even enable automatic processing of the images. Different codes are used to identify the same point in the separate images, and the software can recognize these, reference these together from the various images, and solve for camera locations based on these coded targets. Once enough coded targets are identified to solve for the camera positions, non-coded targets (such as plain dots) can be automatically identified and referenced between the different photographs.

The difficulty in the application of photogrammetry to a brownout cloud, or any other non-traditional object, comes from the complexity of introducing clearly-defined targets, both coded and non-coded, to the images. This necessitates an intensive process of manually studying the images and identifying similar features in the images. For this research, there was no reasonable way to saturate the dust cloud with particles that would be retroreflective and to use coded targets that would be large enough for the cameras to identify at the large distances encountered.

Experimental Setup

The flight testing took place during September 2009 at the US Army YPG Oasis Landing Zone (LZ), a 1000' by 945' area located in the isolated northern section of YPG. Oasis LZ is shown in Figure 3, looking north from the roof of the ground test complex. The aircraft used was the US Army Aeroflightdynamics Directorate's EH-60L Advanced QuickFix aircraft, powered by two General Electric T700-GE-701C turboshaft engines and manned by the test pilot, co-pilot/safety pilot, and flight test engineer.

Figure 3. Oasis LZ, looking north from the roof of the ground test complex

The flight testing occurred in the morning shortly after sunrise to allow for the best overall environmental conditions. According to the climatology report, at 0815 local time (approximate time of the brownout event analyzed), the average temperature was 73.7°F, with an average relative humidity of 19.9%, average pressure of 968.9mb, and average wind speed of 2.5kts at 220° with a max gust of around 11 kts. Figure 4 shows an aerial view of the northern section of the LZ, with the aircraft having landed and the cloud starting to disperse. The meteorological sensor suite was located on a trailer in lane 6 of the LZ as identified in Figure 4. The climatology data sampling rate was every fifteen minutes and the corresponding data is shown in Figure 5. It should be noted that the two peaks for maximum wind speed between 0800 and 0900 are likely caused by the presence of the aircraft approaching the landing zone during this time period. Elsewhere in the data where the maximum wind speed peaks, there is a corresponding increase in the average wind speed. However, this increase in average wind speed does not occur between 0800 and 0900 and remains low at around two to three knots, indicating the wind gusts were not sustained.

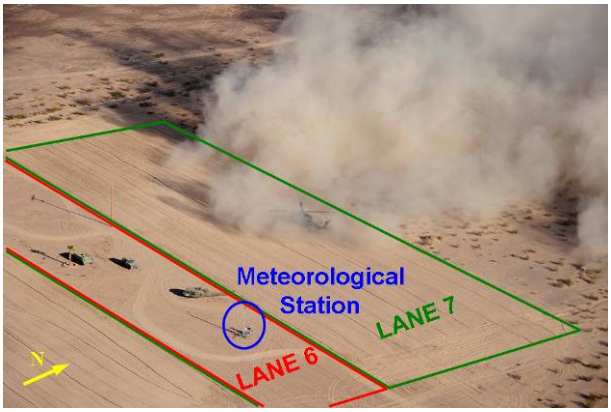

Figure 4. Lane 6 and 7 at Oasis LZ

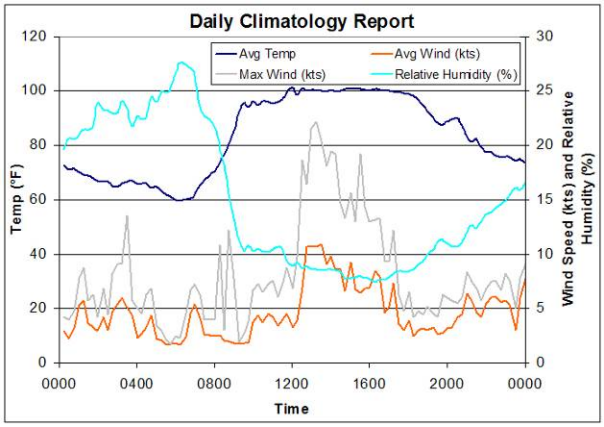

Figure 5. Temperature, wind and relative humidity

Oasis LZ was set up such that there were seven lanes running east-west, all of varying widths, as shown in Figure 6. The four odd-numbered lanes were flying lanes, shown as green in the figure. These were prepared with a tractor-pulled disc harrow to break up the sand, which resulted in a talcum powder-like consistency of the sand to better replicate the unprepared LZs the warfighter experiences in theater. Figure 3 shows lane 5 being prepared by the tractor, with lane 1 (in the foreground) and lane 3 already having been prepared. The remaining even-numbered lanes contained a variety of obstacles used to assess the obstacle-detection capabilities of the prototype onboard aircraft sensors being flight tested, and are represented

as red and yellow zones in the diagram. Lane 7 was used for all of the events throughout the flight test, as this allowed for the pilot to always have an obstacle-free zone on the starboard side of the aircraft if he needed to abort during a brownout landing attempt.

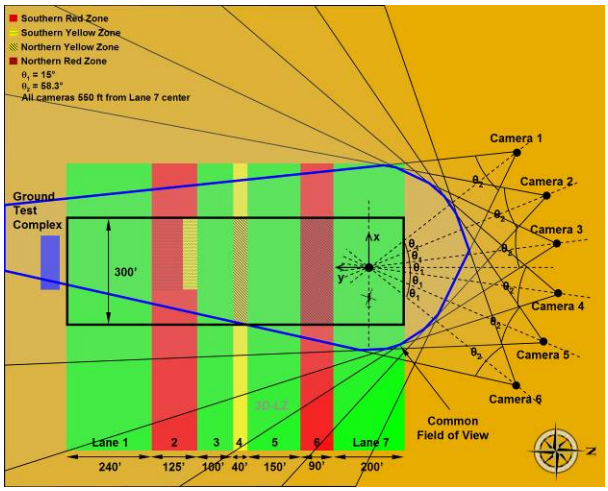

Figure 6. Schematic of Oasis LZ and camera setup

The brownout cloud data was collected using six 15.1 megapixel digital SLR cameras equally spaced about a 75° arc 550' north of the center of Lane 7, as shown in Figure 6. Each of the cameras used a 20mm focal-length lens, giving a 58.3° field of view for the APS-C sized image sensors.

Oasis LZ Soil Samples

A battery of tests were performed on a sample of sand from the LZ in order to get a more complete picture of the nature of the soil at Oasis and to aid in developing the data set fully for future code validation by others. The sample was taken from different locations within lane 7, to a depth of approximately three inches. This was done after it had been prepared with the disc harrow, and the sample was comprised of an accurate representation of the different particle sizes that the soil contained. The sample used for the particle testing was an approximately even mixture of sand taken during the first round of testing in early August 2009 and the second round in late September 2009.

A dry dispersion laser light scattering test was performed on two different samples taken from the larger sample in order to gain information on particle size distribution. The results of this test are given in the particle size distribution plot in Figure 7 and the cumulative distribution plot in Figure 8 and were based on volume, as opposed to mass or number. The figures show the results from two different trials, which was done for repeatability, along with the average of the two. The smallest particles encountered at Oasis were on the order of 2 to 3µm, with only about 3% of particles smaller than 10µm. Roughly 26.4% of particles were between 10 and 100µm, 67.6% between 100µm and 1mm, and just around 3% of particles between 1 and 1.45mm. The highest concentration of particles was found in the 478.6 to 549.5µm range, with a volume percentage of 5.67%, which corresponding to the peaks for both samples in Figure 7. The volume-weighted mean particle size was approximately 328µm, and the median was about 245.8µm, as indicated by the 50% volume mark in the cumulative distribution plot shown in Figure 8. Ten percent of particles fell under 34.2µm, and 10% of particles were larger than 755.7µm. This test also found that the specific surface area, or the total area of particles divided by the total weight, to be $0.088 m^2/g$, and a surface weighted mean, or mean diameter for the surface area, of 68.192µm.

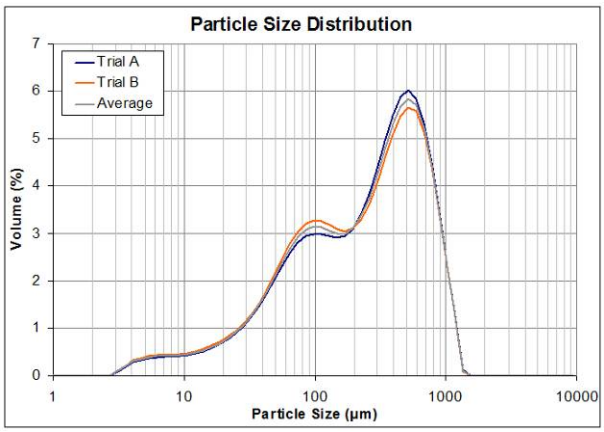

Figure 7. Oasis LZ sample particle size distribution plot

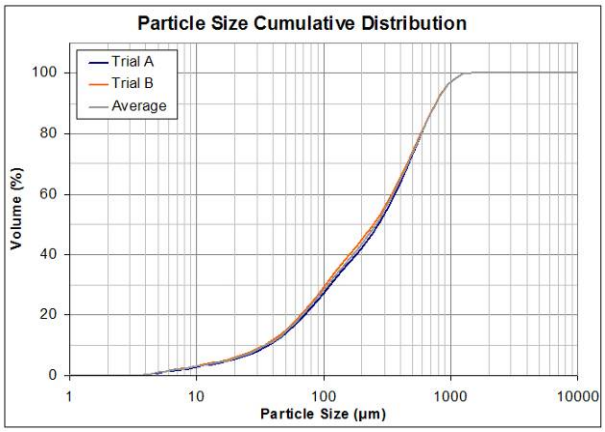

Figure 8. Oasis LZ sample particle size cumulative distribution plot

According to Reference 6, long-term suspension particles in the upper part of the cloud are those with sizes less than 20µm. For the sand at Oasis LZ, this

suggests that only about 6% of the surface particles are entrained in the cloud for a significant length of time. This same figure identifies the short-term suspension particles being in the range of 20 to 70µm, corresponding to approximately 15% of the particles in the sample. This suggests that almost 80% of the surface particles in an LZ are not affected during the evolution of the brownout cloud.

A skeletal density test using helium pycnometry was also carried out for ten cycles on the sample. This found that the average density of the sand was 2.5996g/cm^3 with a standard deviation of 0.0004g/cm^3.

The final test conducted on the sample was a scanning electron microscopy/energy dispersive x-ray spectrometry (SEM/EDS) test, performed with a JEOL JSM-6490LV scanning electron microscope coupled to a Thermo Scientific Noran System SIX energy dispersive x-ray spectrometer system. An image collected from the SEM/EDS test is shown in Figure 9. The numbered areas in the image denote regions where the EDS spectra were collected from individual particles. This test revealed that the sand was comprised primarily of silicon (Si), oxygen (O), carbon (C), aluminum (Al), calcium (Ca), potassium (K), and iron (Fe). Figure 10 shows the overall composition from the entire area in Figure 9, as well as the composition of the particles identified by the numbered areas. A sub-sample of the sand was examined by polarized light microscopy (PLM) to characterize the major mineral types found in the sand, and this indicated the presence of quartz, plagioclase, feldspar, mica, carbonate, clinoamphibole, magnetite, clay and plant fragments.

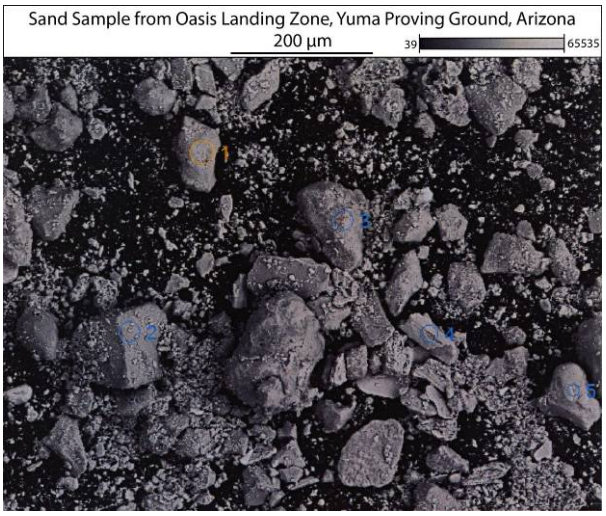

Figure 9. Backscattered electron image of particles comprising sand sample from YPG

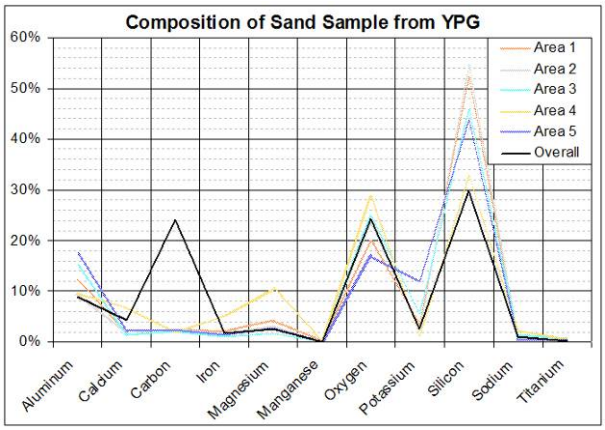

Figure 10: Elemental composition of entire area and numbered areas in Figure 9

Brownout Cloud Characterization

In the previous photogrammetric study detailed in reference 22, two brownout events were examined; one high-speed taxi pass event and one approach to touchdown event. The first event analysis used a temporal resolution of two seconds between frames for a total of six frames and ten seconds of the event. The second used a resolution of two seconds between frames for the first four and last two frames, and between five and six seconds for the other three frames, for a total of eight frames and 25.3 seconds of the event. Even though the data was captured at three frames per second, this decreased temporal resolution was used such that data on the brownout cloud could be obtained over a wide range of time as a first attempt at the analysis and to see if the technique was practicable. It should also be noted that individual points in the images were not tracked between frames, as the temporal resolution was not fine enough to permit this to be done.

The goal of the current study was to look at an approach to touchdown brownout event and focus in on a shorter length of time, but using a higher temporal resolution between frames, the full three frames per second at which the data was captured. This would enable the tracking of individual points and features of the cloud as it grew and allow for a more detailed analysis of the brownout cloud evolution. This would also permit approximate cloud growth velocities to be determined. A two-second period of time was selected to look at in greater detail, with t = 0s corresponding to a local time of 8:13:31.321, a period at which the brownout cloud is fully developed and the aircraft is still slightly visible above the cloud. This time of t = 0s corresponds to Frame 156, or the t = 4.00s frame, from the round two brownout cloud approach to touchdown analysis from Reference 22. Figure 11 shows a timeline of the

photogrammetry image capture showing the images taken from camera 2. The times shown in red refer to the work presented in Reference 22, while those in blue are the times and corresponding frames included in the present research.

A new image processing technique was used that allowed for easier identification of like features between frames. This was performed using the glowing edge filter in Adobe Photoshop CS4, with the parameters of 5/14 for edge width, 15/20 for brightness, and 12/15 for smoothness, and then inverting the resulting image. This helped by forming more distinct boundaries within the cloud that could be more easily referenced between the different cameras and frames. This does not introduce any errors or cause a change in pixel location, as the underlying image, and therefore objects within that image, remains in the same position. Figure 12 shows a comparison between the pre-processed and post-processed images at time t = 0s from camera station 2 and shows both the full frame of the image as well as a zoomed-in image showing the brownout cloud in detail.

The photogrammetry processing was performed using the commercial Photomodeler v6 software package. The process of marking each set of six photographs (one per camera) for each frame analyzed is an intensive and time-consuming procedure, as the user must manually examine the images and mark features in the photographs that appear to be identical. This introduces some uncertainty, as the process relies upon the judgment of the user to identify identical points in the cloud.

The review and marking process began with the set of six images for time t = 0s, which are shown in Figure 14 before the images had gone through the processing technique as described earlier. Once the data for the reference point locations for each image was imported, the camera locations relative to one another were known. After this, the user manually examined each image in detail and marked points that were easily identifiable between the different images within the frame set. Once the same point had been marked in at least two images, the software made an estimate as to where that point should be located in the other images of the set. The default location could either be accepted or changed if the algorithms placed the point in an incorrect position. This process of placing points was repeated until all of the identifiable features in the images had been indicated. This led to a total of 83 points marked on the six images for the t = 0s frame. These 83 points included 13 on the aircraft, since it was still visible above the cloud in this particular frame, but didn't include 40 reference points that remained stationary between the frames. For this set of images, the residual of all the points was less than one pixel, which means that the difference between the expected placement of the point and the actual location of the point was within a single pixel of one another. The total error, a statistical measure of the precision of the markings, of the image set was below 0.4 pixels. Any value less than one pixel indicates a data model with marking that is more precise than first assumed by the software[25].

The next step was to compare the images from time t = 0s to those at the next time-step, or t = 0.33s, and to attempt to determine the location of the marked points at that updated instant in time. This is the step that introduces the most error and variability to the analysis, as there is usually no clearly-defined location for the marked points. As an example of this, Figure 15 shows a comparison between the images from camera 1 at time t = 0s and t = 0.33s. Images a) and b) show the pre-processed photos marked, while c) and d) show the post-processed images with the point markings. Detailed in these is an enlarged section of the image, the same location in all four photos, with the marked points visible. The reader can match the numbered points in the first image with those in the latter image. It should be noted that the corresponding number in the latter images is the second of the two numbers for each point, or the number following the colon. The difficulty in precisely tracking individual points can be observed in Figure 15. The problem is lessened for the post-processed images, but it still relies on the user to select the correct points.

This process was repeated for the remaining frames of the two-second time period that was examined, working frame to frame to track the points on the brownout cloud as it evolved. Figure 16 shows the pre-processed, post-marked images taken from camera 2 for all seven frames of the two-second time period. For each set of images, the residual of all the points remained under one pixel and had a total error of between 0.2 and 0.4 pixels.

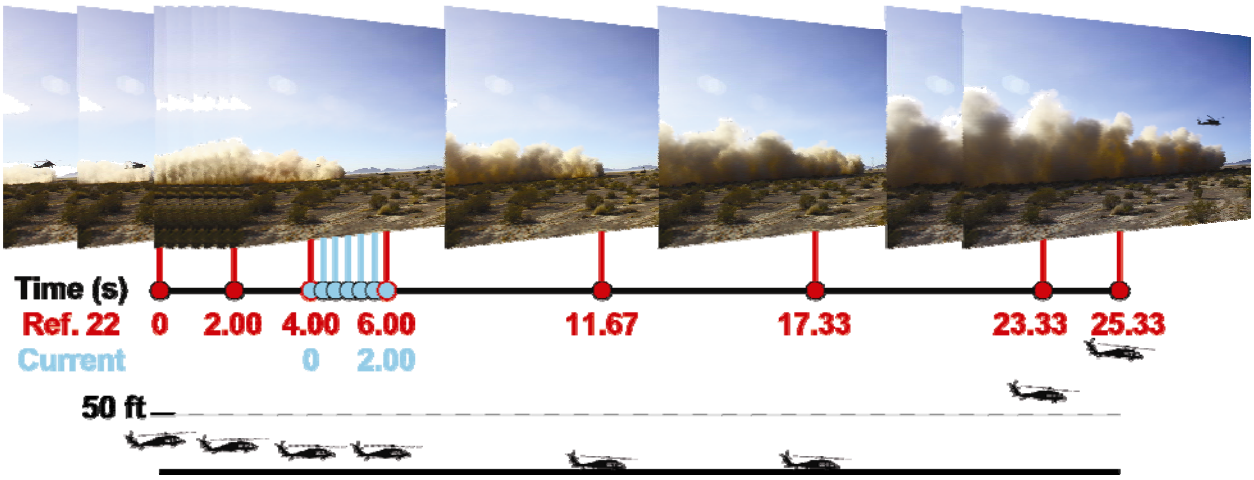

Figure 11. Timeline of photogrammetry image capture, images shown taken from camera 2 at indicated times

a) Full pre-processed image

b) Pre-processed image cloud detail

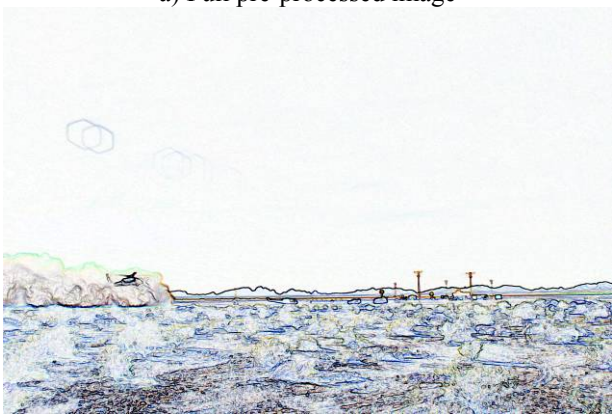

c) Full pre-processed image

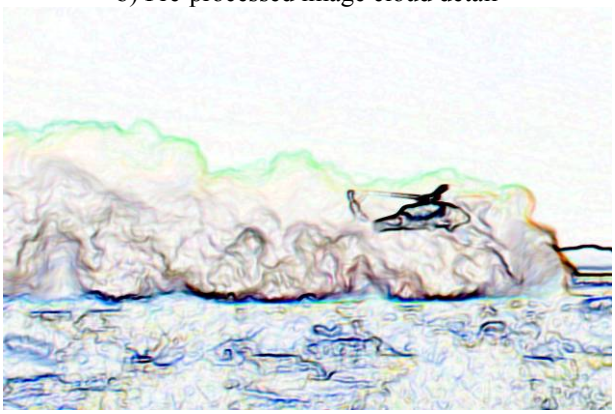

d) Post-processed image cloud detail

Figure 12. Comparison of pre-processed and post-processed images at time t = 0s from camera 2; top images show full frame, bottom images show cloud detail

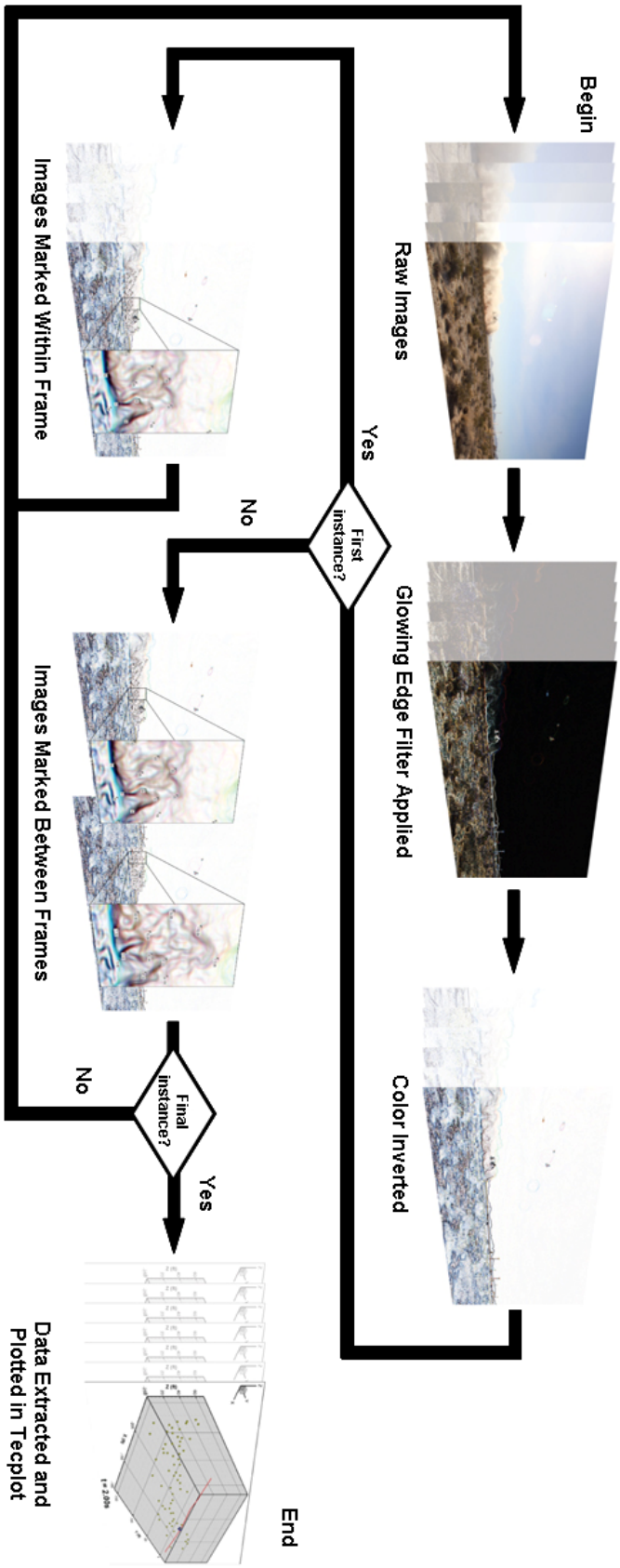

Figure 13. Flow chart of the photogrammetry analysis process

Camera 1, time t = 0s

Camera 2, time t = 0s

Camera 3, time t = 0s

Camera 4, time t = 0s

Camera 5, time t = 0s

Camera 6, time t = 0s

Figure 14. Views from all cameras at time t = 0s before image processing and marking

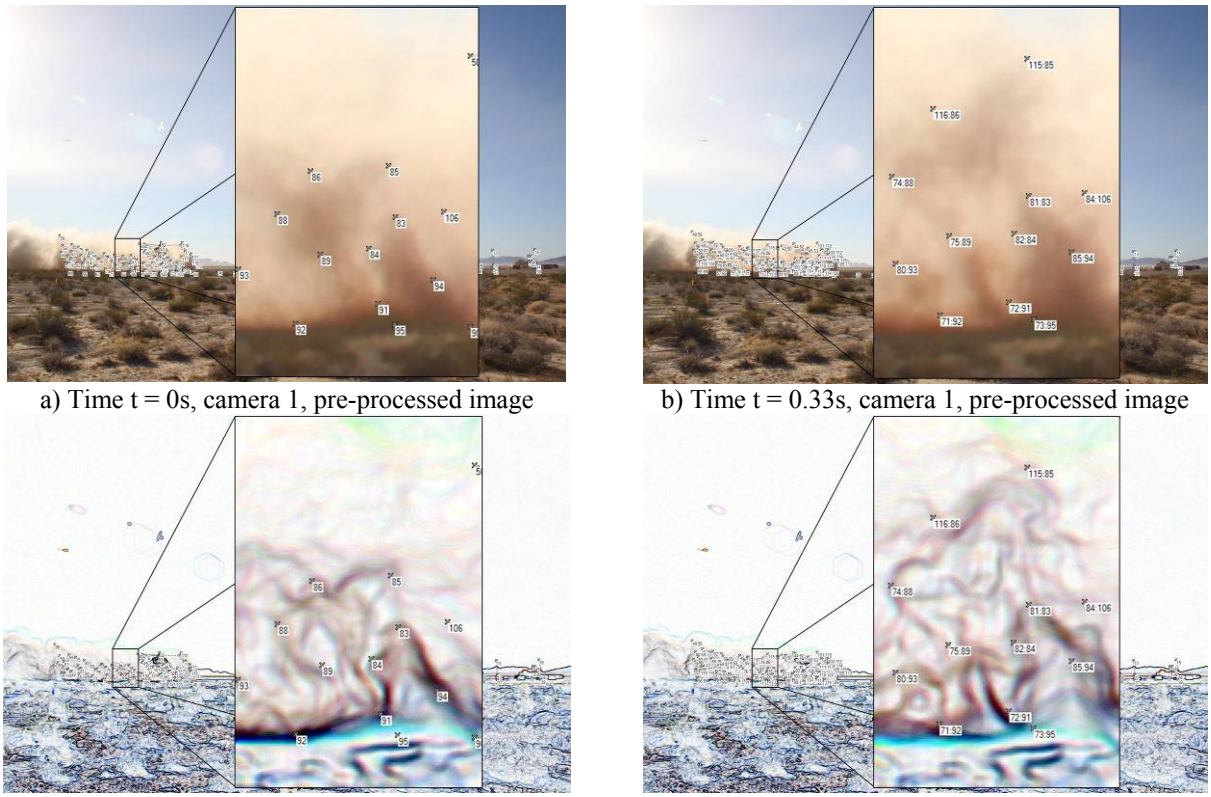

Figure 15. Comparison of pre-processed and post-processed images after marking similar points in photogrammetry software; note in t = 0.33s images, point identification number to match to point in t = 0s images is trailing number

After all of the images for the seven instances had been analyzed, the point data was extracted. This point data was used as the boundary of the brownout cloud and plotted in Figure 17 through Figure 19. The yellow dots in the figures represent the marked points on the brownout cloud, the blue octahedron is the aircraft location (based on the on-board measurement instruments), and the red line shows the aircraft flight path during the approach to touchdown maneuver within the defined spatial region. Figure 17 shows isometric views of the data at the different frame time steps, while Figure 18 shows side views and Figure 19 shows top-down views of the same data set. The three velocity components for each point were solved for by taking the distance traveled between each frame and dividing by the time between frames, which was 0.333s for all cases, and the root sum of squares was used to calculate the velocity magnitude of each point. These velocities are represented in the aforementioned figures by the vectors on each point, scaled to 33.3% of the actual value, and shown in units of ft/s.

From the plots of the point data and the respective velocity vectors, the reader can observe a variety of qualitative characteristics of the cloud. From the top-down view in Figure 19, the points are generally all moving in a radial direction away from the aircraft early on. However, as early as t = 0.33s, there starts to be some movement of points close to the front of the cloud almost perpendicularly to the flight path of the aircraft. This could be due to some of the mixing caused by the interactions from the bundling of tip vortices mentioned in Reference 6. By time t = 1.00s, the majority of the points further away from the aircraft have slowed their outward movement, and referring to Figure 18, are generally moving upward as the cloud is growing. The aircraft is traveling at a ground speed of about 17-18ft/s through the two seconds of this analysis, and mostly in the positive-x direction. Figure 18 also shows the high forward velocities of the points close to the front of the cloud starting at time t = 0s as the aircraft outwash is pushing the cloud forward. A number of these points have velocity components in the x-direction of 35-45ft/s, more than twice the ground speed of the aircraft. The number of points moving entirely in the outward direction begins to decrease by time t = 1.00s, as many of these have started moving upward as well.

Camera 2, time t = 0s

Camera 2, time t = 0.33s

Camera 2, time t = 0.67s

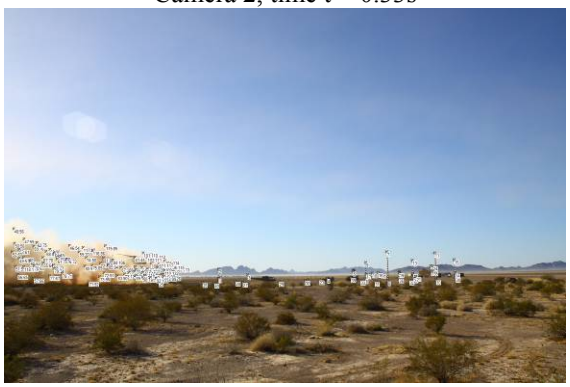

Camera 2, time t = 1.00s

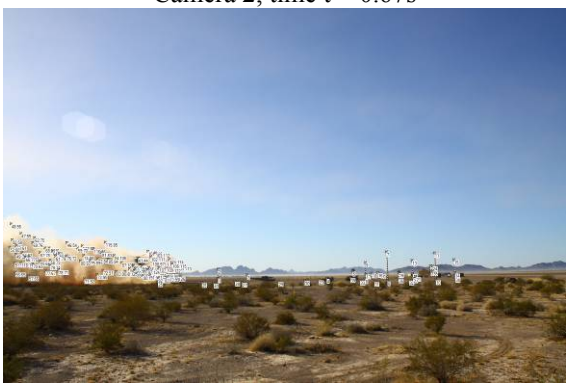

Camera 2, time t = 1.33s

Camera 2, time t = 1.67s

Camera 2, time t = 2.00s

Figure 16. Brownout cloud analysis with pre-processed, marked images for camera 2 through two-second time period

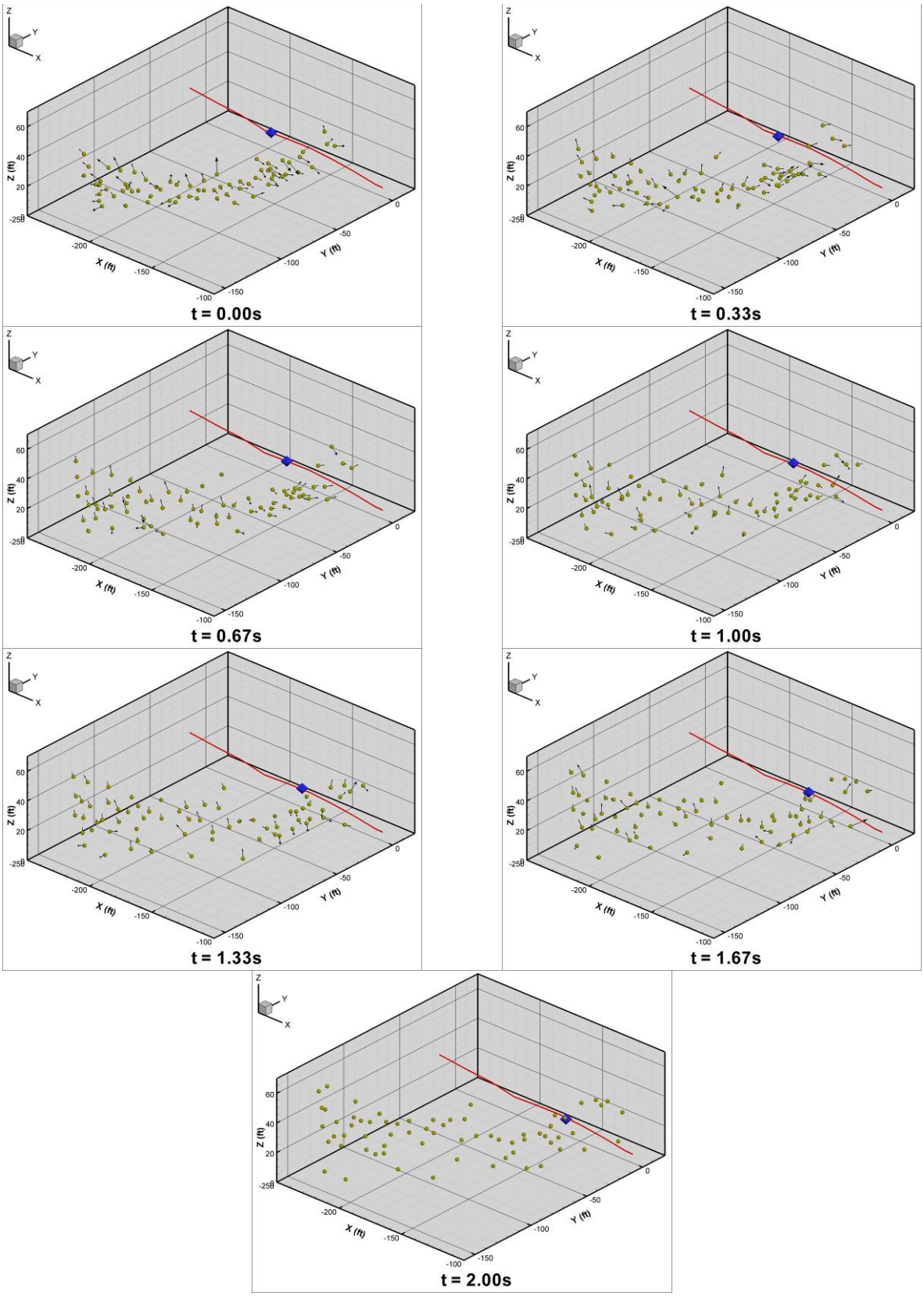

Figure 17. Isometric views of brownout cloud analysis data

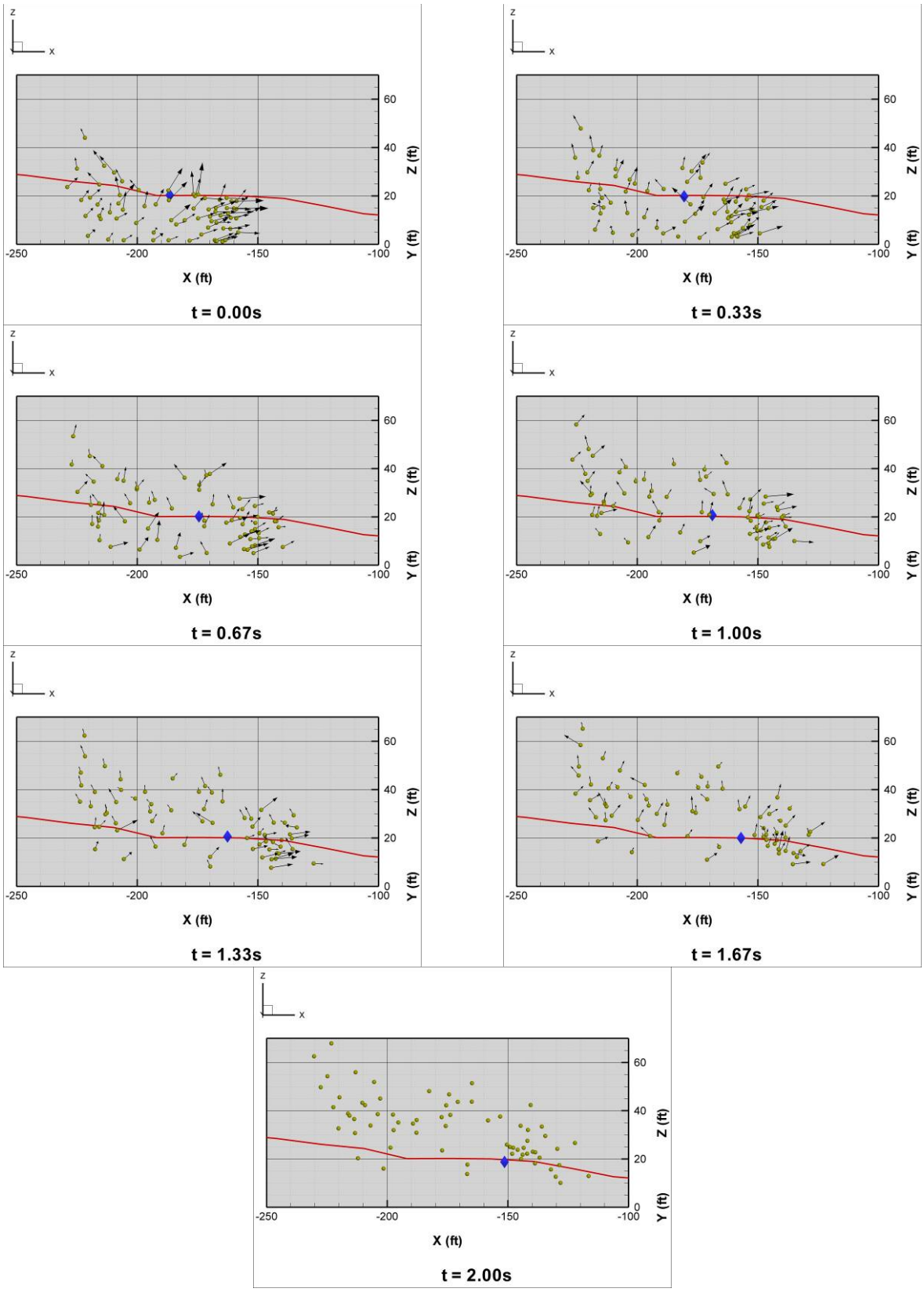

Figure 18. Side views of brownout cloud analysis data

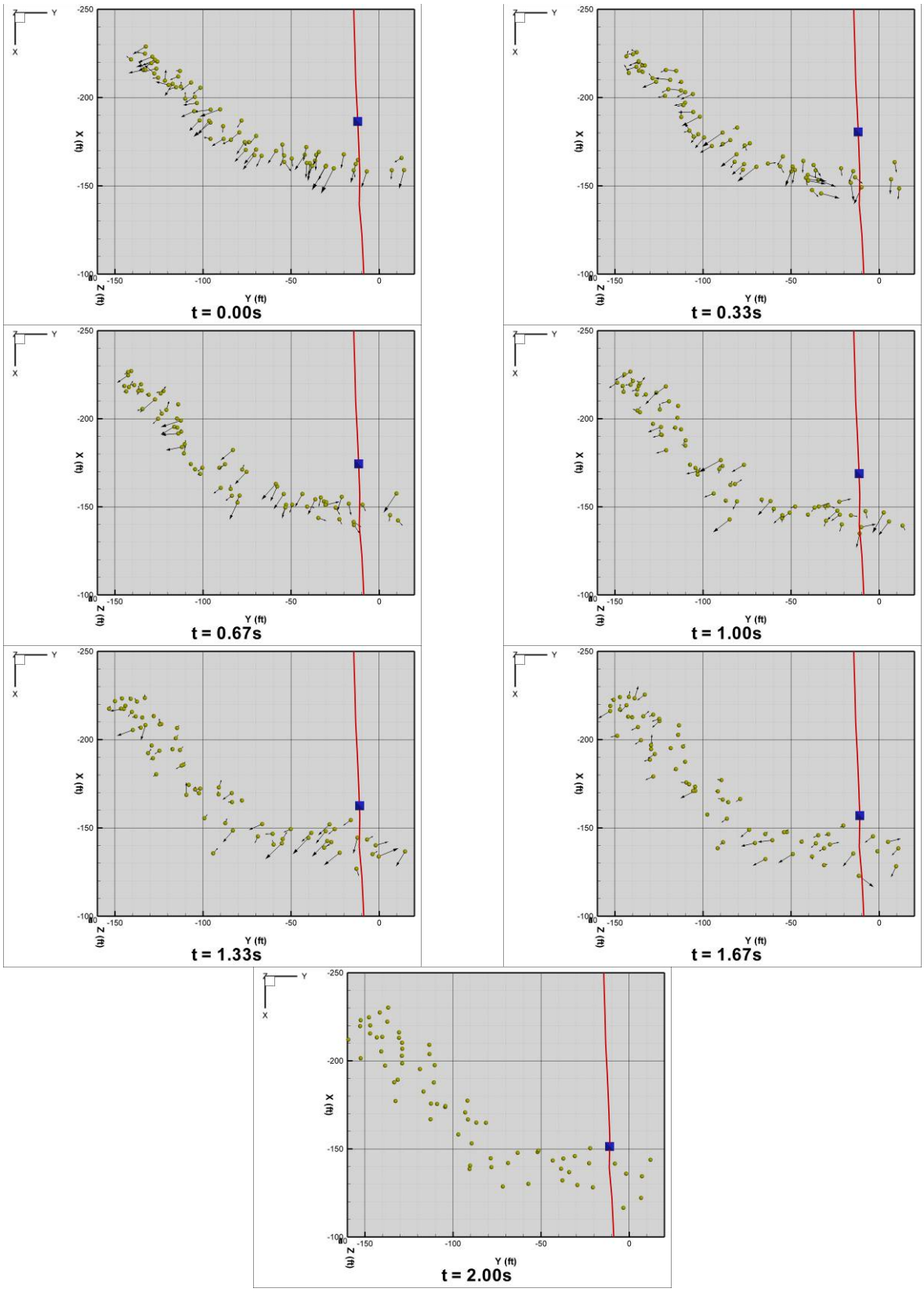

Figure 19. Top-down views of brownout cloud analysis data

The velocity profiles of the cloud are beneficial to examine. The row of points closest to the surface of the LZ at time t = 0s is shown highlighted in red in Figure 20. The velocity magnitudes of these points are shown in Figure 21. Generally speaking, the velocity magnitude of the points further away from the front of the cloud, or the lower numbered points and solid lines in Figure 21, starts out at t = 0s with a high velocity and slow down by the end of the time window examined. Conversely, the points closer to the front of the cloud (the dashed lines), and thus closer to the aircraft's downwash, begin with a lower velocity that usually ends with a higher velocity. This could be because the points further away have already been accelerated by the induced flow and are starting to decelerate as they rise, while the points closer to the front are still in the "initial" phase of the brownout cloud evolution.

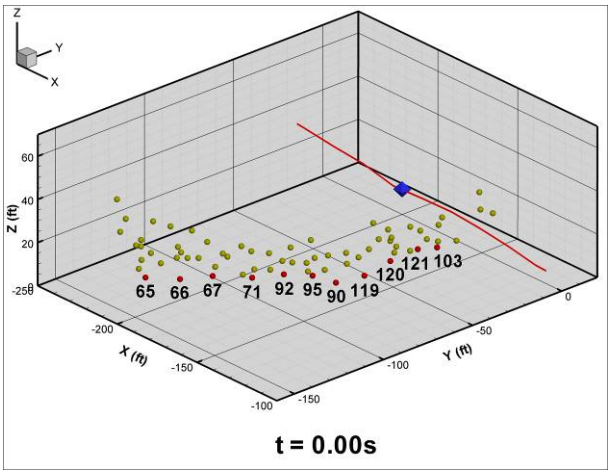

Figure 20. Brownout cloud point identification numbers

Also notable to mention are the columnar structures that form in the cloud, which can be easily seen in the aerial image taken from the testing of the EH-60L landed in lane 7 at Oasis LZ in Figure 23. These structures are much easier to identify looking down on the cloud as in the figure, but are still visible when looking from eye-level, especially when viewing the cloud formation real-time. Using the photogrammetry point data, an approximate size for these columns can be determined. Figure 22 shows the post-processed image, enlarged to focus on the brownout cloud, from camera 2 at time t = 1.67s. This image highlights the column-like structures in the cloud between the red lines, assigning an identification number for each, and their respective dimensions are given in Table 1.

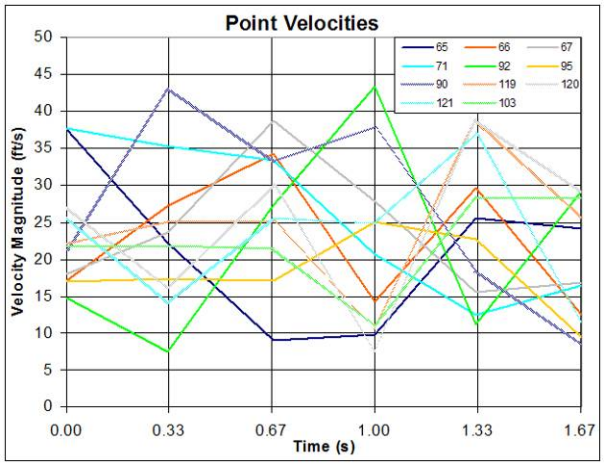

Figure 21. Velocity magnitudes of points initially closest to surface of LZ

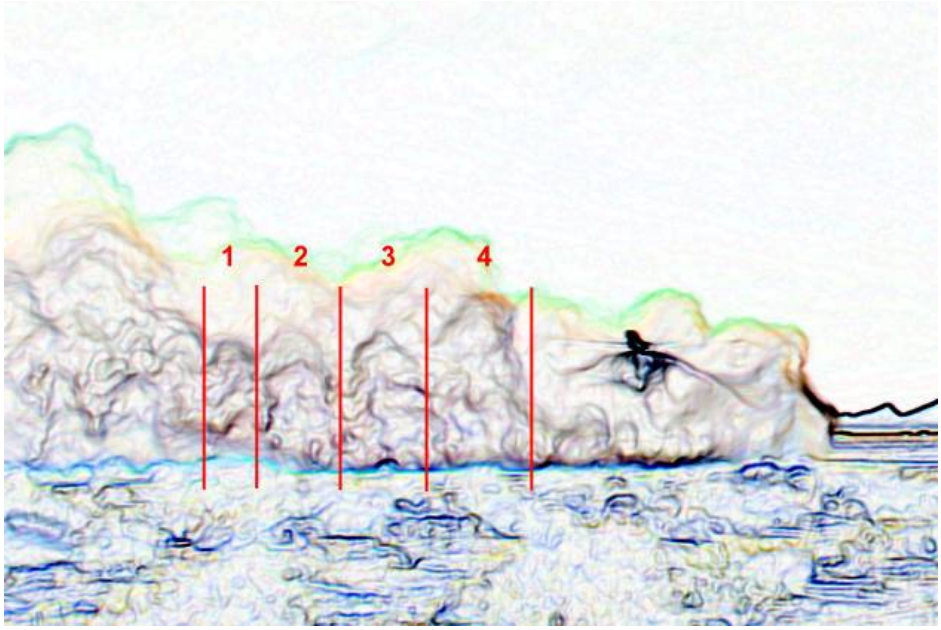

Figure 22. Enlarged view of brownout cloud from camera 2 at t = 1.67s with column-like structures indicated

Table 1. Dimensions of column structures in Figure 22

Column ID	Width (ft)	Height (ft)
1	11	30
2	16	26
3	15.5	32.5
4	16.6	40.5

Figure 23. View of EH-60L touched down at Oasis LZ

Conclusions

The photogrammetry technique developed previously was used for a case with a higher temporal resolution and an improved (yet still subjective based on the user) method of processing the images to enable easier feature identification on the brownout cloud. With this technique, quantitative and qualitative characteristics of a brownout cloud formed during an EH-60L approach to touch down were obtained. A two-second period of time, during which the cloud was fully developed, was analyzed with the images taken at three frames per second. This allowed individual points on the cloud to be tracked frame to frame, which enabled the velocity components of the points on the cloud to be determined. It was found that the points all move generally in a radial direction at first, and the points close to the front of the brownout cloud have high forward velocities as they are being propelled by the rotorcraft outwash. Distinct columnar structures in the brownout cloud were observed at certain times and the dimensions for these at t = 1.67s were obtained.

Particle testing was performed on a sample of sand from the flight test in order to gain a more thorough understanding of the soil. Among other things, this found that the average volume-weighted particle size was around 328μm. Previous research suggests that only about 20% of the particles at Oasis LZ are small enough to be affected by the rotor downwash and outwash. This also found that the sand was mainly composed of silicon, oxygen, carbon, aluminum, calcium, potassium, and iron.

The process of identifying similar points in the brownout cloud between images within the same frame and between images from the same camera at different times proved to be a difficult task. This was due to the non-traditional application of photogrammetry, where there is no solid, stationary object that can be marked easily with targets. However, acceptable values for the point residuals and the total error for each instance in time were still able to be obtained.

Improvements could still be made to the setup used in this research. All six of the cameras used were at the same elevation. It would greatly improve the accuracy of the results, not only by having a different capture angle, but also to help ease the process of identifying similar points between the images. The same number of cameras could still be used, as images from the first three or four cameras were beneficial to the marking process, but the last two cameras had such a rearward view of the brownout cloud that it was difficult to make out any feature on the cloud. These two cameras could be moved to an elevated, forward location, although this would present other difficulties with how to place these at elevation so as not to cause another distraction to the already taxed pilots. It is hoped that this data could be used to help validate brownout prediction codes, with the intent of further understanding the phenomenon of brownout and the dangerous DVE that results from it.

Acknowledgements

The author would like to acknowledge the following individuals for their contributions to this research: Oliver Wong, AFDD JRPO, for his assistance with the testing; Walt Harrington, AFRL, for providing the opportunity to participate in the test; Tom Jones and Benny Lunsford, NASA LaRC, for their guidance in developing the photogrammetry system and technique; and Wayne Mantay and Preston Martin, AFDD JRPO, for their encouragement and suggestions in documenting this work.

References

[1] Colby, S., "Military Spin: Help With Brownouts," Rotor & Wing, March 2005.

[2] Lee, T.E., Leishman, J.G., and Ramasamy, M., "Fluid Dynamics of Interacting Blade Tip Vortices with a Ground Plane," American Helicopter Society 64th Annual Forum, Montréal, Canada, 29 April – 1 May 2008.

[3] Phillips, C., and Brown, R.E., "Eulerian Simulation of the Fluid Dynamics of Helicopter Brownout," Journal of Aircraft, Vol. 46, No. 4, pp 1416-1429, July-August 2009.

[4] "Sandblaster," *Special Operations Technology*, Vol. 4, Issue 7, October 2006.
[5] Acquisition and Technology Programs Task Force, Department of Defense Aviation Safety Technologies Report, Defense Safety Oversight Council, Office of the Under Secretary of Defense for Personnel and Readiness, Washington, DC, 30 April 2009.
[6] Syal, M., Govindarajan, B., and Leishman, J.G., "Mesoscale Sediment Tracking Methodology to Analyze Brownout Cloud Developments," American Helicopter Society 66th Annual Forum, Phoenix, Arizona, 10-13 May 2010.
[7] Wadcock, A.J., Ewing, L.A., Solis, E., Potsdam, M., and Rajagopalan, G., "Rotorcraft Downwash Flow Field Study to Understand the Aerodynamics of Helicopter Brownout," American Helicopter Society Southwest Region Technical Specialists' Meeting, Dallas-Fort Worth, Texas, 15-17 October 2008.
[8] Warwick, G., "Dusting Off," Aviation Week and Space Technology, 5 May 2008.
[9] Harrington, W., Savage, J., McKinley, R.A., Braddom, S., Szoboszlay, Z., and Burns, H.N., "3D-LZ Brownout Landing Solution," American Helicopter Society 66th Annual Forum, Phoenix, Arizona, 10-13 May 2010.
[10] Rodgers, S.J., "Evaluation of the Dust Cloud Generated by Helicopter Rotor Downwash," USAAVLABS Technical Report 67-81, March 1968.
[11] Wenren, Y., Walter, J., Fan, M., and Steinhoff, J., "Vorticity Confinement and Advanced Rendering to Compute and Visualize Complex Flows," 44th AIAA Aerospace Sciences Meeting and Exhibit, Reno, Nevada, AIAA-2006-0945, 9-12 January 2006.
[12] Weible, J., "Visible: A Cure for Brownouts," *Defense News*, 26 January 2009.
[13] Croft, J., "Canadians Demonstrate Brownout Vision Aid," *Flight Global*, 28 April 2009.
[14] Sabbagh, L., "Flying Blind in Iraq: U.S. Helicopters Navigate Real Desert Storms," *Popular Mechanics*, 3 October 2006.
[15] Haehnel, R.B., Moulton, M.A., Wenren, Y., and Steinhoff, J., "A Model to Simulate Rotorcraft-Induced Brownout," American Helicopter Society 64th Annual Forum, Montréal, Canada, 29 April – 1 May 2008.
[16] Phillips, C., and Brown, R.E., "The Effect of Helicopter Configuration on the Fluid Dynamics of Brownout," 34th European Rotorcraft Forum, Liverpool, United Kingdom, 16-19 September 2008.
[17] Wachspress, D.A., Whitehouse, G.R., Keller, J.D., McClure, K., Gilmore, P., and Dorsett, M., "Physics Based Modeling of Helicopter Brownout for Piloted Simulation Applications," Interservice/Industry Training, Simulation and Education Conference (I/ITSEC), Orlando, Florida, No. 8177, 1-4 December 2008.
[18] Johnson, B., Leishman, J.G., and Sydney, A., "Investigation of Sediment Entrainment in Brownout Using High-Speed Particle Image Velocimetry," American Helicopter Society 65th Annual Forum, Grapevine, Texas, 27-29 May 2009.
[19] D'Andrea, A., "Unsteady Numerical Simulations of Helicopters and Tiltrotors Operating in Sandy-Desert Environments," American Helicopter Society Specialists' Conference on Aeromechanics, San Francisco, California, 20-22 January 2010.
[20] Nathan, N.D., and Green, R.B., "Wind Tunnel Investigation of Flow Around a Rotor In Ground Effect," American Helicopter Society Specialists' Conference on Aeromechanics, San Francisco, California, 20-22 January 2010.
[21] Wachspress, D.A., Whitehouse, G.R., Keller, J.D., Yu, K., Gilmore, P., Dorsett, M., and McClure, K., "A High Fidelity Brownout Model for Real-Time Flight Simulations and Trainers," American Helicopter Society 65th Annual Forum, Grapevine, Texas, 27-29 May 2009.
[22] Wong, O.D., and Tanner, P.E., "Photogrammetric Measurements of an EH-60 Brownout Cloud," American Helicopter Society 66th Annual Forum, Phoenix, Arizona, 11-13 May 2010.
[23] Liu, T., Cattafesta, L.N., Radeztsky, R.H., "Photogrammetry Applied to Wind Tunnel Testing," AIAA Journal, Vol. 38, No. 6, pp 964-971, June 2000.
[24] "The Basics of Photogrammetry," Geodetic Services Inc., available from: http://www.geodetic.com/v-stars/info.asp?whatis, accessed 3 February 2011.
[25] "Photomodeler 6 Help File," Eos Systems Inc., distributed with Photomodeler 6, accessed 13 November 2009.